International Journal of Electrical and Electronics Engineers
Volume 16, Issue No. 02, July-Dec 2024
ISSN (O) 2321-2055
ISSN (P) 2321 -2045

A THREE-DIMENSIONAL ELECTRICAL IMPEDANCE TOMOGRAPHY POST-PROCESSING METHOD

Mohd. Faisal[1], Dr. Pushpneel Verma[2], Dr. Ramesh Kumar[3]

[1]Department of Computer Science & Engineering, College of Engineering & Technology, BU Ajmer, Rajasthan, India,
m_faisalcse@rediffmail.com

[2]AP, Department of Computer Science & Engineering, College of Engineering & Technology, BU Ajmer, Rajasthan, India,
pushpneelverma@gmail.com

[3]AP, Department of Electrical & Compter Engineering, Government Engineering College, Ajmer, Rajasthan, India,
rameshkumarmeena@gmail.com

ABSTRACT

The Modern biomedical imaging techniques include electrical impedance tomography. The objective is to capture images of human tissue's electrical characteristics. This non-invasive method has no known risks and is safe for the patient's health. That being said, the method's accuracy is poor. Due of their excellent noise resilience, linear inverse solvers find widespread use in medical applications. The solution that corresponds to a linear perturbation from an initial estimate can only be approximated by linear methods. A unique reconstruction method is suggested in this work. With the intention of replicating the sharp change in conductivity at the boundaries between tissues or organs, a nonlinear approach is used to post-process the conductivity distribution following the application of a linear solution. The suggested strategy is contrasted with three other popular ways using the results. The suggested technique significantly lowers the error associated with picture reconstruction while providing images of higher quality and more robustness against noise.

KEYWORDS

Electrical Impedance Tomography, Human Tissues, noise resilience, linear inverse solvers

1. INTRODUCTION

This document describes, and is written to conform to, author guidelines for the journals of AIRCC series. It is prepared in Microsoft Word as a .doc document. Although other means of preparation are acceptable, final, camera-ready versions must conform to this layout. Microsoft Word terminology is used where appropriate in this document. Although formatting instructions may often appear daunting, the simplest approach is to use this template and insert headings and text into it as appropriate.

The imaging method known as electrical impedance tomography (EIT) is mostly employed in biomedical imaging[1]. By applying an electrical current at the volume's boundary and measuring the resulting potential

International Journal of Electrical and Electronics Engineers
Volume 16, Issue No. 02, July-Dec 2024
ISSN (O) 2321-2055
ISSN (P) 2321 -2045

there, one can estimate the electrical impedance within a volume conductor [2]. Since the electrical properties of various biological tissues vary, EIT can be used in biomedical imaging. Even though EIT was first discussed in the 1970s [3], it is actually a relatively new technology since the high-quality, reasonably priced hardware, strong algorithms, and computational resources needed to address the challenge are still in their infancy [4].

Since an EIT inverse issue is extremely ill-posed and highly nonlinear [5], its solution is typically not trivial and requires an initial estimate of the conductivity distribution [6]. This inverse problem has been solved by a number of approaches, each with pros and cons. To put it briefly, those techniques can be divided into four different classes: machine learning (ML)-based techniques [12], direct nonlinear techniques [11], nonlinear iterative techniques [10], and linear approximation [9]. The conductivity distribution is estimated using linear methods as a tiny deviation from a first estimate [13]. The reconstruction technique can more accurately approximate a good solution to the inverse issue by assuming an initial conductivity distribution, for example, by applying a regularisation approach or prior distribution. Unlike linear methods, nonlinear algorithms do not heavily depend on an initial guess and have the potential to achieve higher accuracy in theory. Nonlinear methods, however, are less dependable in the majority of biomedical applications [14] because they are more susceptible to electrode displacements, modelling mistakes, and time-varying contours of the imaged region. Even while more precise reconstructions can be made using prior probability functions [15] in the presence of noisy data, the inverse issue is still ill-posed for these techniques, and even tiny modelling errors can result in significant distortions in the image [16].

Artificial neural networks, or ANNs, are AI algorithms that can find a more accurate approximation of a nonlinear problem's solution [17]. Applications of EIT inverse problems have demonstrated ANNs' rapidity in solving the inverse problem [18]. But because ANNs are built on machine learning, it seems difficult to provide accurate training data for practical biomedical applications [10]. The primary flaw in ANNs is that they cannot estimate and extrapolate solutions from data that hasn't been seen before. The latter is the main disadvantage of using ANNs to biomedical settings to tackle the EIT inverse problem. Since modelling errors and noise are not negligible in real clinical data, it is not possible to train an algorithm to simulate the conductivity distribution since noise cannot always be assessed beforehand.

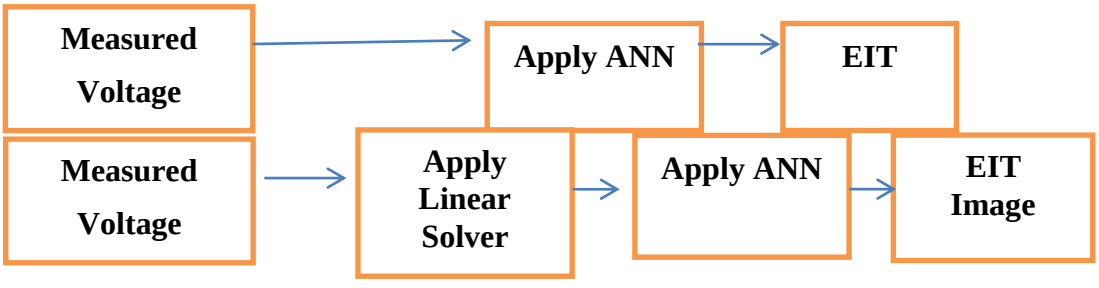

EIT Comparison of the suggested approach with (a) current ANN-based reconstruction techniques.

In this paper, a new method for handling a three-dimensional EIT problem is presented. In order to combine the benefits of both linear approximations and nonlinear optimisations, this method combines both linear

International Journal of Electrical and Electronics Engineers
Volume 16, Issue No. 02, July-Dec 2024
ISSN (O) 2321-2055
ISSN (P) 2321 -2045

approximations and an ANN in the inverse problem. A linear distribution is obtained after using the linear one-step Gauss-Newton (GN) algorithm [19] to solve the inverse problem. The plan is to employ an artificial neural network (ANN) as a post-processing technique to correct the conductivity distribution and get over the inverse solver's shortcomings. A significantly higher level of noise robustness should be obtained by applying the ANN after resolving the EIT inverse problem. While modelling noise and potential distortions in the measured voltages is necessary when applying an ANN directly to the data, this intensive modelling is not necessary when applying the ANN to the output of a linear reconstruction algorithm to produce a good image. Since the linear algorithms are actually well-known for being incredibly noise-resistant, the resulting conductivity distribution is not significantly impacted by the modelling mistakes when contrasted with the measured voltages. Therefore, instead of using an ANN as an image reconstruction processor, training an ANN as a post-processor to improve the reconstruction quality should give a stronger robustness to measurement errors present in the measured data, even if they are not taken into account during the training phase. Figure 1 compares the suggested approach with current ANN-based solutions that are currently in use.

Three popular approaches are compared to the suggested method: an inverse solver based on an ANN [21], a linear method [19], and a nonlinear iterative method [20]. The outcomes demonstrate the efficiency, stability, and speed of the suggested strategy.

2. RESULT: PHANTOM EXPERIMENT

The following formatting rules must be followed strictly. This (.doc) document may be used as a template for papers prepared using Microsoft Word. Papers not conforming to these requirements may not be published in the conference proceedings.

Ionised water was filled in a cylindrical tank for phantom tests. After inserting two acrylic electrical insulators inside the phantom, data on the EIT test was gathered. The proposed post-processing method, an ANN utilised as an inverse solution, an iterative primal dual interior point method (PDIPM) solver, and a linear one-step GN were the four different approaches used to conduct EIT image reconstruction. Figure 2 displays cross-sections of the final photos, while Extended Data Figure 1 displays the 3D models. The fnite element (FE) model's border is in close proximity to the expected position, however the linear one-step GN approach accurately yields two distinct targets adjacent to it. The conductivity distribution becomes smoothed out by the linear approach, making it challenging to accurately represent the two goals without producing noticeable errors. The existence of the blue colour in the reconstruction is caused by the underlying algorithm's smoothness, which tends to produce huge ringing artefacts. It is highly possible that these distortions will cause the conductivity distribution to be interpreted incorrectly.

The iterative PDIPM approach, denoted by the green cylinders in Fig. 2(b), accurately displays two distinct targets at the intended location. In comparison to the linear one-step GN, the ringing artefacts, represented by the blue objects in the figure, are much reduced when a nonlinear method is used since it does not provide a smooth conductivity distribution. In Figs. 2(c) and (e), the EIT inverse problem is solved via the application of an ANN.

International Journal of Electrical and Electronics Engineers
Volume 16, Issue No. 02, July-Dec 2024
ISSN (O) 2321-2055
ISSN (P) 2321 -2045

Image reconstruction from noisy data may result in significant mistakes if the artificial neural network (ANN) is trained without taking into account the noise that will inevitably be present in the measured data. The reconstruction produced from phantom data using such an ANN is displayed in Figure 2(c). The ANN produces deformed shapes instead of the two predicted cylindrical objects, although without producing any obvious ringing faults. This subpar picture reconstruction was predicted by the theory and by prior research, which shown that ANNs are both highly sensitive to modelling mistakes and noise in the observed data and capable of executing a decent reconstruction. A satisfactory reconstruction is provided by the conductivity distribution that this ANN was able to obtain. The predicted positions of the two distinct items, which are represented as two electrical insulators, appear to coincide with the original position. Moreover, there are no ringing artefacts or obvious distortion.

Using the same measurement data, the proposed technique—which combines the linear reconstruction method with ANN—was evaluated. The ANN was trained using EIT reconstructions from the one-step GN solver, which were acquired using simulated data, in the suggested approach. The suggested post-processing technique and an ANN trained without taking noise in the measured data into account were used to create the image in Figure 2(d).

The suggested approach outperformed an ANN utilised as an inverse solver trained without taking noise in the measurement data into account, as seen in Fig. 2(c). The image was only slightly affected by the poorly modelled and continuously fluctuating electrode positions, contact impedance, and model contours [22] when the inverse problem was solved using a linear approach, such as the one-step GN. However, for the suggested post-processing technique, training the ANN without taking into account the noise in the measured data still produced a good image that was comparable to the image produced by an ANN trained with noisy measurement data.

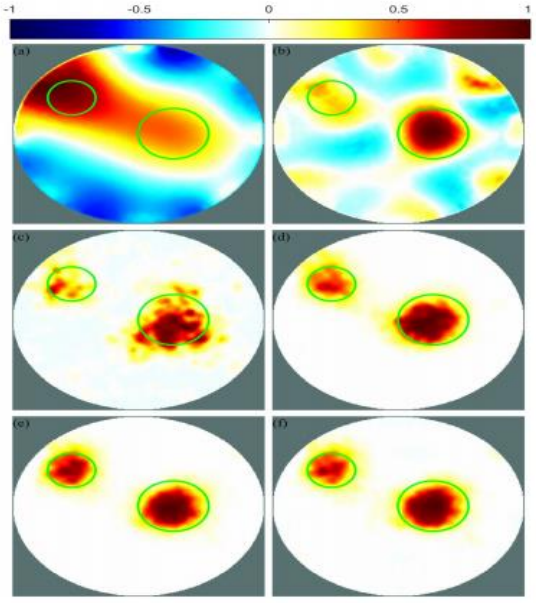

Figure 2: Cross-sectional view of EIT reconstructions using various techniques using phantom data One-step GN (a), PDIPM (b), ANN as inverse solver trained without taking noise into account (c), ANN as inverse solver

International Journal of Electrical and Electronics Engineers
Volume 16, Issue No. 02, July-Dec 2024
ISSN (O) 2321-2055
ISSN (P) 2321 -2045

trained with noisy data (e), ANN as inverse solver trained with noisy data (f), and suggested post-processing method and ANN trained with noisy data (d). The targets' locations are indicated by green circles. The normalised conductivity distribution is represented by the top bar.

In order to lessen the need for extrapolation by the ANN, noise was added to the simulated voltage data for the final reconstruction, which is depicted in Fig. 2(f). This made the voltages more similar to the voltages measured from the phantom. This strategy produced a similar image when compared to the suggested post-processing method and an ANN trained on noise-free data. The two targets are visible where they should be. The human eye cannot see the smoothness, ringing effects, or shape deformation. When the ANN was used as a post-processing technique, it produced a satisfactory reconstruction free of ringing artefacts and smoothness, in contrast to the ANN that was utilised as an inverse solver trained from noisy voltages. Furthermore, unlike what could occur with linear approaches, the generated images demonstrate that the two rebuilt objects did not shift towards the boundary of the FE model.

Method	**PE #1 (%)**	**PE #2 (%)**	**|ΔRES| (%)**	**SD (%)**
One-step GN	2.69	2.30	19.44	20.03
PDIPM	1.95	2.10	8.10	22.91
ANN (training: no noise)	2.60	1.76	6.90	17.87
One-step GN + ANN (training: no noise)	1.35	0.55	2.59	11.21
ANN (training: noise)	0.97	0.37	2.35	10.35
One-step GN + ANN (training: noise)	1.01	0.50	2.27	10.55

Table 1 shows the PE, |ΔRES|, and SD errors that were found when reconstructing from phantom data using various techniques. Fig. 2 displays corresponding images. On the left side of the images is target #1, and on the right side is target #2.

To verify the visual impression that the suggested post-processing using ANN provided a considerable resistance to the noise present in the measurements, different errors23 were computed for each reconstruction. Table 1 presents the corresponding mistakes. Position error (PE) denotes a mistake in the target's position. PE was split into two mistakes, one for every distinct target. The left target in the Fig. 2 photos is referred to as the first target, while the right target is referred to as the second target. The FE model's radius is used to normalise PE inaccuracies. The one-step GN approach tended to push the reconstruction for the first target nearer the FE model's boundary, increasing the PE—which in this case reached 2.69%. As demonstrated in Fig. 2(c), the ANN employed as an inverse solver that was trained without taking noise into account produced a subpar outcome with a PE of 2.60%. ANN-based techniques yielded a PE of less than 1.35%, whereas other methods demonstrated remarkable accuracy in estimating the target's position. The ANN employed as an inverse solver trained without noisy data and the linear one-step GN produced the two highest PE for the second target, much like the first target did. When trained without taking noise into account, the ANN utilised as an inverse solver trainer produced an error of 1.76%, but the one-step GN produced an error of 2.30%. With an inaccuracy of

International Journal of Electrical and Electronics Engineers
Volume 16, Issue No. 02, July-Dec 2024
ISSN (O) 2321-2055
ISSN (P) 2321 -2045

0.37%, the best estimate was produced by an ANN that was trained with noisy data and utilised as an inverse solver. Less than 0.2% greater than the ANN employed as an inverse solver trained with noisy data, post-processing techniques did not surpass 0.55% (obtained with training without noise).

The difference between the target's and the reconstructed object's areas can be understood as the difference of resolution (|ΔRES|) errors. huge smoothness was produced via the one-step GN approach, resulting in a huge |ΔRES| of 19.44%. When trained with the presence of noise, the suggested strategy yielded the lowest error, at 2.27%. An ANN utilised as an inverse solver produced a low error of 2.35% when trained appropriately. On the other hand, the inaccuracy rose to 6.90% if the ANN was not trained appropriately. The suggested post-processing produced a low error in all scenarios, irrespective of whether noise presence was taken into account during training (2.27%) or not (2.59%). As can be observed from Extended Data Fig. 1, additional |ΔRES| errors acquired at different heights of the 3D model are shown in Extended Data Table 1. These errors demonstrate that the suggested technique performed better than previous methods at different cross-sections.

Likewise, 20.03% and 22.91%, respectively, were the big shape deformation (SD) errors obtained by the linear one-step GN technique and PDIPM. An artificial neural network (ANN) utilised as an inverse solution yielded an extremely low error of 10.35% when trained taking noise in the measurements into account. In the absence of such, the SD error may reach 17.87%. While training the ANN with noisy voltages consistently produced somewhat better results, training the ANN without taking the noise into account also produced a low error rate using the suggested post-processing strategy. Here, the standard deviation changed by less than 1%, from 10.55% with noisy data during training to 11.21% with clean data. This observation demonstrates the suggested method's great stability and robustness against noise.

In summary, Table 1 demonstrates that the suggested approach can provide a correct reconstruction of the EIT inverse problem without requiring a deep understanding of the data collecting equipment beforehand.

The one-step GN solver's computational cost is made up of a straightforward matrix product. It takes 3,029.18 seconds and 48.6GB of memory to compute the matrix. Nevertheless, the matrix can be computed prior to resolving the inverse problem since it is independent of the measurements. When using the one-step GN solution in this example, the reconstruction matrix was taken into consideration as known.

Table 2 lists the amount of time and memory needed to solve the EIT inverse problem using various techniques. Using the one-step GN method, the EIT inverse problem could be handled in 0.1 seconds with only 0.6GB of data after the reconstruction matrix was known. In order to accomplish a reconstruction, the iterative PDIPM method needs a lot of memory and time. The issue is solved by this solution in 4,289 seconds and 65.46 GB of memory, but it converges to an exact reconstruction. In this case, the ANN-based inverse solver method took the shortest time—just 0.36 seconds and 0.38 GB. The suggested approach requires more time than these two solvers since it combines a one-step GN solver with an ANN. In this case, the ANN-based inverse solver method took the shortest time—just 0.36 seconds and 0.38 GB. The suggested approach requires more time than these two solvers since it combines a one-step GN solver with an ANN. Here, the suggested approach required just 1.1GB of memory to solve the inverse problem in 0.80 seconds.

While the PDIPM can also solve the EIT problem very accurately, fast imaging applications cannot use this solution because of its iterative nature, which takes time and resources. The iterative PDIPM strategy requires

International Journal of Electrical and Electronics Engineers
Volume 16, Issue No. 02, July-Dec 2024
ISSN (O) 2321-2055
ISSN (P) 2321 -2045

more than 100 times the amount of memory to solve the inverse problem and is over 4,000 times slower than the suggested post-processing solution. This means that costly hardware must be used, which is a significant disadvantage.

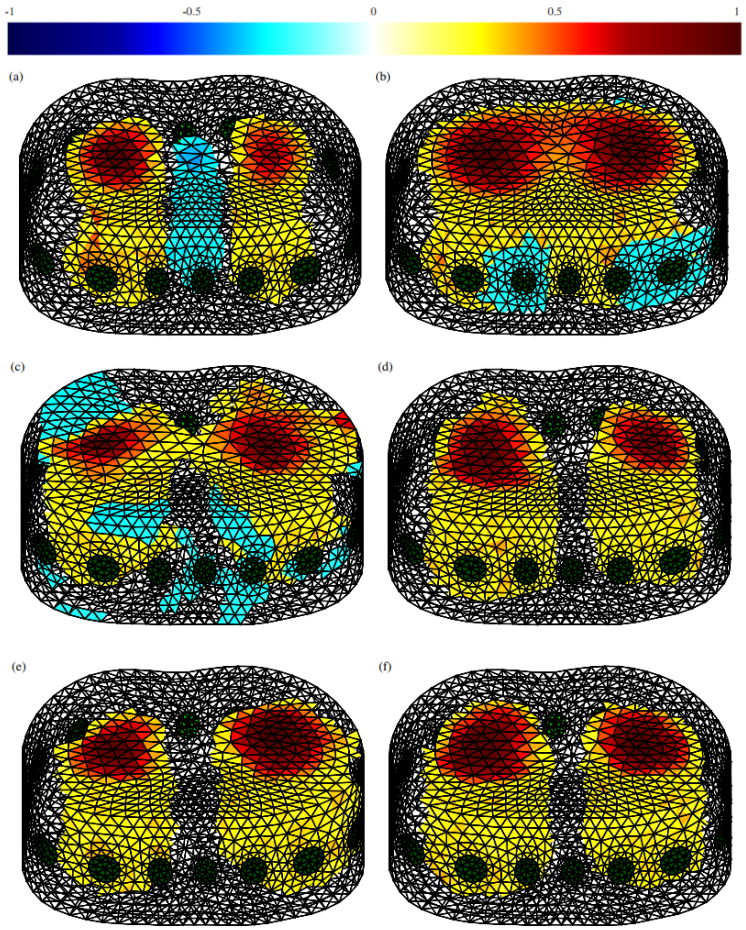

Figure 3 shows the 3D EIT reconstructions of lung data using various techniques: one-step GN, PDIPM, ANN as inverse solver, trained by taking into account sources of errors, proposed method, trained by taking into account errors in measurement data, ANN as inverse solver, trained without taking into account errors, and proposed post-processing method, trained without taking into account errors. The distribution of normalised resistivity is provided at the top. In green are the electrodes.

Lung data.

The EIT data of a healthy individual were gathered24, and the same four techniques were used to rebuild the images. In this experiment, the subject's chest was surrounded by 16 electrodes in a single plane. Two comparable elliptical forms were anticipated to represent the lungs because the person was in good health. The conductivity patterns inside the FE models created from lung data using various techniques are displayed in Figure 3. Extra Information A cross-section from these FE models is displayed in Fig. 2. Extra Information The conductivity distribution at the electrode location, in the middle of the FE model, is depicted in Fig. 2.

The one-step GN approach, which is commonly employed in real-time biomedical applications, produced a picture that showed two distinct targets, but it also included some smoothness and artefacts, which reduced the

quality of the reconstructed image. There were discernible ringing artefacts between the two lungs. These artefacts, which are shown as the blue area in Fig. 3(a), had to be removed since they may have caused the practitioner to interpret the results incorrectly and make an inaccurate diagnosis.

While the plots in Figs. 3(c–f) depict divided lungs, the PDIPM result in Fig. 3(b) depicts a fused lung. When compared to Fig. 3(a), the accepted standard, Fig. 3(c) is distorted and Fig. 3(e) is slightly deformed. Furthermore, Figs. 3(d) and (f) are far better than Fig. 3(a) and the remaining plots in Fig. 3.

The outcome of employing an ANN as an inverse solution was highly dependent on the simulated data that was used to train the ANN. In general, the better the outcome, the closer they were to the measured data. This comment suggested that a significant amount of modelling work would be needed to train an ANN to produce outstanding EIT picture reconstruction. Since this study examined time-distance EIT, the modelling required to take into account movement and model distortion with time, which resulted in electrode displacement, in addition to the patients' breathing activities. Additionally, studies have indicated that modelling efforts should take hardware-dependent noise in the measured data into account in order to get better results. The reconstruction using an ANN as the inverse solver is depicted in Figures 3(c) and (e). Whereas the ANN is trained by taking into account the existence of such artefacts in Fig. 3(e), it is trained by excluding noise, electrode movement, and model deformations in Fig. 3(c). Since the data were obtained at the conclusion of the inspiration and expiration phases, the image should show two comparable targets that correspond to the conductivity difference during the breathing cycle. Two distinct elliptical zones are seen if the ANN is trained while taking into account the various causes of errors, as in Fig. 3(e). Despite the appearance of the lef lung being slightly smaller than the right, their diameters are rather similar and they are easily distinguishable from one another. However, as shown in Fig. 3(c), when the ANN is trained without taking into account the flaws and inaccuracies of the hardware, significant artefacts may arise, shapes may not match expectations, and it may become difficult to distinguish between the two distinct regions.

Regarding the phantom studies, the suggested approach demonstrated reduced sensitivity to disturbances, motion, and mismeasurements. Images obtained using the suggested method are shown in Figures 3(d) and (f), respectively, by taking into consideration and not taking into consideration the various sources of mistakes during the training phase. The two lungs are distinguishable and visible in both situations. While there are some artefacts in Fig. 3(d), where the ANN is trained without taking into account any source of measurement error, the reconstruction's visual quality is noticeably better than that of the reconstruction based only on the ANN, as seen in Fig. 3(c). In contrast to the other nonlinear methods employed in this work, the suggested approach produced noticeably fewer artefacts.

At last, the best representation of the conductivity difference in the lungs during the breathing cycle can be found in Fig. 3(f); the image shows no discernible artefact, two huge symmetrical forms, and low smoothness. However, this phase was not required to create a good image of two different targets identical to the lungs, even though taking modelling mistakes into account during the ANN's training enhanced the outcome. This finding helps significantly lower the modelling effort needed to train an ANN effectively for biological applications.

The computer resources required for 3D EIT reconstruction were measured for each approach. The iterative PDIPM approach is slow and unsuitable for real-time monitoring, but generally providing high quality. The

one-step GN- and ANN-based approaches are significantly faster than the PDIPM method. On a CPU, the suggested method can solve the inverse problem in less than 0.3 seconds, and on a GPU or other specialised hardware, it should be even faster. Table 3 displays CPU time and memory usage.

Different measurements were made during the breathing cycle, and each unique image was reconstructed to demonstrate the stability of the suggested method. The outcomes can be found in Extended Data Figs. 3–6. Despite the stability of the one-step GN approach, the pictures display relatively tiny lungs with ringing artefacts in between. The PDIPM technique produces high-quality images, but when the reference and measured signals are obtained at the same time as the breathing cycle (i.e., the end of expiration), it also produces huge artefacts instead of blank images. Although the ANN utilised as an inverse solver produced odd forms that were different from the expected shape of the lungs, it seemed stable. Ultimately, a precise and durable reconstruction was provided by the suggested approach. The generated images display two lungs of similar size and a good shape that is similar to the shape acquired from other imaging modalities, such as computed tomography, during a whole breathing cycle.

3. CONCLUSIONS

This research proposes a new reconstruction technique for 3D EIT. The suggested method combines the benefits of both linear and nonlinear approaches by providing near real-time image reconstruction, significant robustness against noise, and rough boundaries. While simulation results do not demonstrate a significant improvement over the current ANN-based methods, the new approach described in this research clearly shows improvements in phantom and lung data, particularly in producing high-quality images from noisy environments. Prior to using the ANN, solving the EIT issue with linear solvers helps to lower the influence of noise in the measured data and increases the stability of the nonlinear ANN. Because of its increased stability, an ANN may be trained to solve the EIT inverse problem using biomedical data without requiring a deep understanding of the hardware or human anatomy's physiology. The suggested strategy offers significantly more stability and increased robustness to previously unseen data when compared to a solution based solely on an ANN. The results demonstrate that using the suggested strategy, training an ANN capable of producing a high resolution image no longer requires a thorough understanding of the data gathering technology or the anatomy of the patient.

This discovery means that the computationally intensive training process only needs to be completed once, after which any patient and any EIT hardware on the market can use the same set of weights and biases. In this work, CPU computations were made and Matlab was used to tackle the inverse difficulties. The authors think that real-time implementation of a high-quality, stable, and non-linear EIT image reconstruction of the lungs should be possible thanks to advancements in computer technology and a GPU-based implementation of the suggested technique.

Methods

A real phantom provided the phantom data. Electrodes were arranged in four layers within the cylindrical tank. There were eight distinct electrodes in each layer, for a total of 32 electrodes. neighbouring current patterns were employed for both current injection and measurements, which meant that every pair of electrodes used

matched two neighbouring electrodes on the same layer. Tu25's data collecting technology was utilised to obtain phantom data. This system injects current into each pair of two neighbouring electrodes that are on the same layer. 32 different voltages were measured for each current injection using the 32 pairs of neighbouring electrodes that were present at the volume conductor's boundary. After that, the current source moved to the next set of nearby electrodes, and 29 more measurements were taken. Ultimately, the picture reconstruction process included 928 measurements.

The challenge posed by practical EIT applications is accurately simulating the volume conductor's shape and the electrode locations. The true boundary shape varies somewhat across patients and is constantly changing as they breathe, which affects the monitoring process. Additional inaccuracies arise from the electrode placing because of the occurrence of flaws in measuring the contour of the thoracic region. Additionally, a reconstruction in a fixed FE model can only provide an approximation answer because of movement that occurs during data capture between the measurement of the reference signal and the actual frame. It is well known that nonlinear iterative techniques are quite sensitive to the mismatch between the real volume conductor shape and the boundary of the FE model.

Using two different sets of measurements, often obtained at two different times, and taking into account the difference between these two measurements to perform the reconstruction is known as the difference EIT technique. This method aids in mitigating errors resulting from imprecise models. But only one FE model is needed to picture the conductivity distribution in the inverse situation. Put another way, the difference EIT may only aid in reducing the mistakes caused by imprecise modelling; it cannot completely eliminate them if the volume conductor's shape changes while the measurement is being made.

It has been demonstrated that when educated appropriately, ANNs are capable of handling these problems. In order for an artificial neural network (ANN) to be trained to take into account modelling errors that may arise in real-world biomedical applications, the training data must contain these kinds of aberrations. Different FE models have to be used to address the forward problems in order to train the ANNs from simulated data in this study. Fourier coefficients of the typical human thorax were used to create and deform a circular FE model for the EIT imaging of the lung data. In order to achieve various thorax-like shapes during the training phase, the Fourier coefcients were altered with a random weight of up to 10% of the original coefcient. Furthermore, two distinct FE models were employed to address the forward problems in the homogeneous and inhomogeneous instances, respectively, in light of the work's emphasis on difference EIT. Afterwards, other models were used to tackle the forward difficulties. Ultimately, the inverse problem for the suggested post-processing solution was resolved in a FE model of the lungs that was obtained without changing the Fourier coefficients.

The suggested approach was contrasted with two commonly used techniques for EIT reconstructions of the lungs as well as a reconstruction method that just used an ANN.

EIT inverse solvers.

Newton's gauss in one step. A popular direct linear reconstruction technique for real-time imaging applications is the one-step GN26. This approach has the benefit of not requiring iteration, which allows for the quick computation of the inverse problem's solution. This reconstruction approach, named after the mathematicians

International Journal of Electrical and Electronics Engineers
Volume 16, Issue No. 02, July-Dec 2024
ISSN (O) 2321-2055
ISSN (P) 2321 -2045

Carl Friedrich Gauss and Isaac Newton, can be understood as a simplified linearized version of the nonlinear GN method. Actually, the nonlinear method's first step is the only one that is computed. This approach provides a quick and satisfactory reconstruction since, in the difference EIT, several of the full nonlinear method's parameters have very low identifiability and may thus be adjusted to constant values.

The Technique of primal-dual interior points.

Since the nonlinear PDIPM reconstruction method is iterative, estimating an answer to the inverse problem needs a significant amount of time and processing power. In both linear and nonlinear programming, barrier approaches are the fundamental foundation of Te PDIPM. Anthony V. Fiacco, Garth P. McCormick, and others investigated the concept of encoding the feasible set with a barrier and creating barrier techniques in the early 1960s27. These techniques belong to the class of simplex procedures, where the viable set28's border is followed by the solution. Karmarkar developed a brand-new algorithm known as Karmarkar's algorithm, which is exceptionally effective in real-world applications and executes in provably polynomial time29. This technique, subsequently named the PDIPM, can search at the interior of the feasible set rather than the boundary when compared to the simplex approaches. Later, in 2012, Borsic and Adler suggested solving the EIT inverse problem20 using the PDIPM approach, which produced excellent picture reconstructions with nonlinear conductivity distributions and rough borders. This algorithm was applied in this study using the L2 norm for the regularisation term and the L1 norm for the data.

Originally developed for the Newton one-step error reconstructor (NOSER) algorithm30, the well-known prior probability function was employed with both the one-step GN solver and the PDIPM solver.

Noise estimate

2,000 EIT images with randomly selected targets were simulated in order to train the ANN. The forward and inverse issues were solved for each of these conductivity distributions. There were targets with random conductivity that were distinct from the backdrop in each of the 2,000 EIT photos. The EIDORS toolkit24 and Matlab's neural network toolbox, operating on an Intel Core I7-6700 CPU at 4GHz with 64GB of RAM and Ubuntu Linux, were utilised to obtain solutions for the forward and inverse problems. Once the forward problem was solved, noise was introduced into the voltages that were simulated. By examining the measured signals at the electrodes, the quantity of noise contributed was ascertained.

A tenth-order bandpass filter focused on the injected current frequency was able to remove most of the noise, but some noise remained in the recorded data. It was interesting to train the ANNs with noisy data that was comparable to the data obtained from the phantom in order to lessen the need to extrapolate from the ANNs.

The physical separation between the current source and the measurement electrodes determined the quantity of noise, which was not fixed. Every lung data measurement and phantom experiment has its own noise estimate. A 100 kHz sinusoidal waveform was used for the current injection. Each set of electrodes detected 20 voltages during a sine wave.

These data were filtered, and the largest peak was taken into consideration for the EIT reconstruction. The observed data was then compared to a sine wave simulation to assess the noise. The noise was taken to be a WGN by approximating the level of noise in the measurements prior to filtering. The noise level was calculated using (1):

International Journal of Electrical and Electronics Engineers
Volume 16, Issue No. 02, July-Dec 2024
ISSN (O) 2321-2055
ISSN (P) 2321 -2045

SNR (dB) = 10*log(mean(signal)^2 / Mean(residual noise^2)) (1)

In the end, an average of the signal-to-noise ratios for each of the 928 measurements was calculated over 500 different frames. The estimated SNR was more than 50 dB when the measured signal was located in close proximity to the injected current. The SNR may, however, be less than 10 dB when measured at the other side of the phantom, which is mostly due to the medium's attenuation. It was feasible to replicate the noise by adding a WGN to the generated sine waves by presuming a WGN before filtering. After that, a noise model that approximated the noise found in the actual phantom tests was produced by mimicking the existence of a filter.

Internal organs and movements may also be to blame for the noise levels in the lung tests. Therefore, it was thought to be a non-Gaussian noise. The measured signals' Fourier transform was analysed, and the measurement data was supplemented with non-Gaussian noise.

Artifcial Neural Networks.

The hidden layer of neurons employed radial basis functions (RBFs). The transfer function that was used in the output layer was linear. Studies have demonstrated that this particular ANN configuration can provide high-quality EIT reconstructions from biological data. When using an artificial neural network (ANN) as an inverse solver, the number of neurons in the input layer is equal to the number of measurements (e.g., 208 neurons for the lung data, 928 neurons for the imaginary data). The number of neurons in the input layer for the post-processing application is equal to the number of nodes in the FE model. The hidden layer in this investigation consisted of 1,000 neurons with an RBF transfer function in both scenarios. Ultimately, the output layer included as many neurons as there were nodes in the FE model and produced an estimate of the conductivity distribution inside it.

Training data were simulated in order to train the ANN for the phantom data. One or two cylindrical insulators were simulated to be present in a saline solution in those simulation data. The random electrical conductivity of each insulator was determined to be less than the background. The homogeneous background's electrical conductivity was not constant in those simulations; rather, it changed at random for each training sample. Following up to 2,000 distinct conductivity distribution simulations, the forward problems were solved both with and without taking distortions (movement) into account. To prevent committing the inverse crime, a very fine FE model that differs from the model used to solve the inverse problems and a second-order forward solver were employed while solving the EIT forward problems.

Each lung in the scenario of the lungs was seen as an electrical insulator in relation to the backdrop conductivity. According to research, the lungs' electrical conductivity is stronger at the conclusion of the inspiration phase than it is at the end of the expiration phase. Previous research indicates that the lungs should have an electrical impedance of about 700Ω.m at the frequency of the injected current, or 100 kHz, at the end of expiration. By the time the inspiration phase ends, the electrical impedance should increase to a maximum of 2,500Ω.m. The heartbeat and blood circulation within the body are two other elements that may influence the electrical characteristics of various tissues and materials passed by the electrical current. When a different pair of electrodes is employed for measurement, the difference in conductivity between the two different current injections is predicted to stay minimal and is therefore disregarded throughout the ANN's training. The background impedance in this study was arbitrarily chosen at 700Ω.m. Since differential EIT was employed in

this application, the background conductivity difference ought to have been invisible. Put another way, the spinal cord and blood vessels were invisible in the rebuilt image because there was no change in the conductivity surrounding them between two measurements. Consequently, these artefacts were disregarded when creating the training samples. While blood pressure variations and movement may theoretically be represented in the final image in real biological applications, ignoring them greatly simplifies the process of creating 2,000 training samples. The training of the RBF ANNs involved simulating the presence of two elliptical cylinders with random conductivities and sizes that varied within the range of potential electrical conductivities identified in earlier research. Following training using the particle swarm optimisation technique, the resultant artificial neural network (ANN) presumed the existence of two lungs, which seems a plausible assumption for biomedical imaging. Commonly used techniques for biomedical EIT applications were used to solve the forward and inverse challenges.

Errors.

A consensus called the Grau consensus reconstruction algorithm for EIT, or GREIT, attempted to offer normalised error definitions23. Various functions have been proposed for use as an error function for medical imaging applications31–33. The position error (PE), resolution (RES) error, and shape deformation (SD) were determined among these normalised definitions since they were significant. Although these normalised definitions were created for 2D EIT, they are readily applicable to 3D EIT problems as well. These errors are calculated in 2D EIT using a rasterized picture of the FE model. The study examined the resulting errors on several cross-sections of the Finite Element model. The difference of resolution |ΔRES|18 was employed since it was anticipated that RES would provide an estimate of the target's area.

In the event that the phantom had multiple targets, a PE was calculated using the technique outlined by Martin and Choi21 for each distinct target.

REFERENCES

[1]. Brown, B. H. Electrical impedance tomography (EIT): a review. J. Med. Eng. Technol. 27, 97–108 (2003).

[2]. Bayford, R. H. Bioimpedance tomography (electrical impedance tomography). Annu. Rev. Biomed. Eng. 8, 63–91 (2006).

[3]. Henderson, R. P. & Webster, J. G. An Impedance Camera for Spatially Specific Measurements of the Torax. IEEE Trans. Biomed. Eng. BME-25, 250–254 (1978).

[4]. Hartinger, A. E., Gagnon, H. & Guardo, R. Accounting for hardware imperfections in EIT image reconstruction algorithms. Physiol. Meas. 28, S13–27 (2007).

[5]. Kabanikhin, S. I. Definitions and examples of inverse and ill-posed problems. J. Inverse Ill-posed Probl. 16, 317–357 (2008).

[6]. Holder, D. S. Electrical Impedance Tomography: Methods, History and Applications. (Institute of Physics Publishing, 2005).

[7]. Ramirez T., M. P., Robles G., M. C. & Hernandez-Becerril, R. A. On the computational methods employed in two-dimensional Electrical Impedance Tomography. In 2010 7th International Conference

on Electrical Engineering Computing Science and Automatic Control 274–279, doi:10.1109/ICEEE.2010.5608621(IEEE, 2010).

[8]. Leonhardt, S. & Lachmann, B. Electrical impedance tomography: the holy grail of ventilation and perfusion monitoring? Intensive Care Med. 38, 1917–29 (2012).

[9]. Stephenson, D. R., Davidson, J. L., Lionheart, W. R. B., Grieve, B. D. & York, T. A. Comparison of 3D Image Reconstruction Techniques using Real Electrical Impedance Measurement Data. In 4th World Congress on Industrial Process Tomography, Aizu, Japan (2009).

[10]. Minhas, A. S. & Reddy, M. R. Neural network based approach for anomaly detection in the lungs region by electrical impedance tomography. Physiol. Meas. 26, 489–502 (2005).

[11]. Knudsen, K., Lassas, M., Mueller, J. & Siltanen, S. Regularized D-bar method for the inverse conductivity problem. Inverse Probl. Imaging 3, 599–624 (2009).

[12]. GhasemAzar, M. & Vahdat, B. V. Error Study of EIT Inverse Problem Solution Using Neural Networks. 2007 IEEE Int. Symp. Signal Process. Inf. Technol. 894–899, doi:10.1109/ISSPIT.2007.4458154 (2007).

[13]. Allers, A. & Santosa, F. Stability and resolution analysis of a linearized problem in electrical impedance tomography. Inverse Probl. 7, 515–533 (1991).

[14]. Borsic, A., Graham, B. M., Adler, A. & Lionheart, W. R. B. In vivo impedance imaging with total variation regularization. IEEE Trans. Med. Imaging 29, 44–54 (2010).

[15]. González, G., Huttunen, J. M. J., Kolehmainen, V., Seppänen, A. & Vauhkonen, M. Experimental evaluation of 3D electrical impedance tomography with total variation prior. Inverse Probl. Sci. Eng. 24 (2016).

[16]. Zhou, Z. et al. Comparison of total variation algorithms for electrical impedance tomography. Physiol. Meas. 36, 1193–1209 (2015).

[17]. Hu Hen, Y. & Hwang, J.-N. Handbook of neural network signal processing. (CRC Press, 2001).

[18]. Martin, S. & Choi, C. T. M. Nonlinear Electrical Impedance Tomography Reconstruction Using Artificial Neural Networks and Particle Swarm Optimization. IEEE Trans. Magn. 52, 1–4, doi:10.1109/TMAG.2015.2488901 (2016).

[19]. Brandstatter, B. Jacobian calculation for electrical impedance tomography based on the reciprocity principle. IEEE Trans. Magn. 39, 1309–1312 (2003).

[20]. Borsic, A. & Adler, A. A primal–dual interior-point framework for using the L1 or L2 norm on the data and regularization terms of inverse problems. Inverse Probl. 28, 95011 (2012).

[21]. Martin, S. & Choi, C. T. M. On the influence of spread constant in radial basis networks for electrical impedance tomography. Physiol. Meas. 37, 801–819, doi:10.1088/0967-3334/37/6/801 (2016).

[22]. Lionheart, W. R. B. EIT reconstruction algorithms: pitfalls, challenges and recent developments. Physiol. Meas. 25, 125–142 (2004).

[23]. Adler, A. et al. GREIT: a unified approach to 2D linear EIT reconstruction of lung images. Physiol. Meas. 30, S35–S55 (2009).

[24]. Adler, A. & Lionheart, W. R. B. Uses and abuses of EIDORS: an extensible software base for EIT. Physiol. Meas. 27, S25–S42 (2006).

[25]. Tu, C.-Y. Development of High Resolution Electrical Impedance Tomography System. (National Chiao Tung University, 2015).

[26]. Mayer, M. et al. Direct reconstruction of tissue parameters from differential multi-frequency EIT in vivo. Physiol. Meas. 27, S93–101 (2006).

[27]. Fiacco, A. V. & McCormick, G. P. The Sequential Unconstrained Minimization Technique for Nonlinear Programing, a Primal-Dual Method. Manage. Sci. 10, 360–366 (1964).

[28]. Gonzaga, C. C. Path-Following Methods for Linear Programming. SIAM Rev. 34, 167–224 (1992).

[29]. Karmarkar, N. A new polynomial-time algorithm for linear programming. in Proceedings of the sixteenth annual ACM symposium on Theory of computing - STOC' 84 302–311, doi:10.1145/800057.808695 (ACM Press, 1984).

[30]. Cheney, M., Isaacson, D., Newell, J. C., Simske, S. & Goble, J. NOSER: An algorithm for solving the inverse conductivity problem. Int. J. Imaging Syst. Technol. 2, 66–75 (1990).

[31]. Abascal, J.-F. P. J., Arridge, S. R., Bayford, R. H. & Holder, D. S. Comparison of methods for optimal choice of the regularization parameter for linear electrical impedance tomography of brain function. Physiol. Meas. 29, 1319–34 (2008).

[32]. Birgül, O., Eyüboğlu, B. M. & Ider, Y. Z. Experimental results for 2D magnetic resonance electrical impedance tomography (MREIT) using magnetic flux density in one direction. Phys. Med. Biol. 48, 3485–504 (2003).

[33]. Flores-Tapia, D., O'Halloran, M. & Pistorius, S. A bimodal reconstruction method for breast cancer imaging. Prog. Electromagn. Res. 118, 461–486 (2011).